Integrity Monitoring of LTE Signals of Opportunity-Based Navigation for Autonomous Ground Vehicles

Mahdi Maaref, Joe Khalife, and Zaher M. Kassas
University of California, Riverside

BIOGRAPHIES

Mahdi Maaref received a B.S. and M.S. from the University of Tehran in 2008 and 2011, respectvely, and a Ph.D. in Electrical Engineering from Shahid Beheshti University, in 2016. He was a visiting research collaborator at the University of Alberta, Edmonton, Canada in 2016. Currently, he is a postdoctoral research fellow at the University of California, Riverside and a member of the Autonomous Systems Perception Intelligent and Navigation (ASPIN) Laboratory. His research interests include opportunistic perception, distributed estimation, and real-time systems.

Joe Khalife is a Ph.D. student at the University of California, Riverside and a member of the ASPIN Laboratory. He received a B.E. in Electrical Engineering and an M.S. in Computer Engineering from the Lebanese American University (LAU). From 2012 to 2015, he was a research assistant at LAU. His research interests include opportunistic navigation, autonomous vehicles, and software-defined radio.

Zaher (Zak) M. Kassas is an assistant professor at the University of California, Riverside and director of the ASPIN Laboratory. He received a B.E. in Electrical Engineering from the Lebanese American University, an M.S. in Electrical and Computer Engineering from The Ohio State University, and an M.S.E. in Aerospace Engineering and a Ph.D. in Electrical and Computer Engineering from The University of Texas at Austin. In 2018, he received the National Science Foundation (NSF) Faculty Early Career Development Program (CAREER) award. His research interests include cyber-physical systems, estimation theory, navigation systems, autonomous vehicles, and intelligent transportation systems.

ABSTRACT

A receiver autonomous integrity monitoring (RAIM) framework for autonomous ground vehicle navigation using ambient cellular signals of opportunity (SOPs) is developed. The developed framework considers a ground vehicle navigation exclusively with cellular long-term evolution (LTE) signals and an inertial measurement unit (IMU), without global navigation satellite system (GNSS) signals. A fault detection test is developed to deal with biased LTE pseudorange measurements and a horizontal protection level (HPL) calculation is derived. Experiments to evaluate the developed RAIM framework are presented for a ground vehicle navigating in an urban environment over a trajectory of 1.35 km. It is demonstrated that the RAIM framework detects and excludes biased pseudoranges, reducing the root mean-squared error (RMSE) by 49%.

I. INTRODUCTION

Autonomous ground vehicles (AGVs) require an extremely accurate, robust, and tamper-proof navigation system. Global navigation satellite system (GNSS) receivers are heavily relied upon in current vehicular navigation systems to provide aiding corrections to inertial sensors and to produce an estimate of the vehicle's state in global frame. However, the GNSS navigation solution may become unavailable in deep urban canyons [1] and under unintentional interference and jamming scenarios [2]. One approach to overcome the limitation of GNSS is to exploit ambient signals of opportunity (SOPs). SOPs are radio frequency (RF) signals that are not intended for navigation but can be exploited for navigation purposes, especially in GNSS-challenged environments [3–6]. SOPs include a wide range of signals such as digital television, cellular, and AM/FM radio signals. SOPs are abundant in urban canyons and are free to use, making them desirable sources for navigation, either as a complement or an alternative to GNSS signals. Among the different types of SOPs, cellular signals are particularly attractive due to their favorable

Preprint of the 2018 ION GNSS+ Conference Miami, FL, September 24–28, 2018

geometric configuration, high carrier-to-noise ratio of the received signals, and high bandwidth compared to GNSS signals [7]. In particular, long-term evolution (LTE) signals have a bandwidth up to twenty times higher than that of GPS L1 C/A, which yields better suppression of multipath effects [8, 9]. The recent literature have reported experimental navigation results with standalone cellular signals with meter-level accuracy on ground vehicles [9–12] and centimeter-level accuracy on aerial vehicles [13, 14]. Moreover, it was demonstrated that these signals could provide lane-level accuracy when coupled with a lidar without GNSS signals [15].

As the number of systems that rely on cellular SOPs for navigation grows, the need for monitoring the integrity of cellular-based navigation solutions increases. Integrity monitoring refers to the capability of the system to detect anomalies and warn the user when the system should not be used. A high-integrity navigation system must be able to reject incorrect measurements and provide an integrity metric of the confidence in these systems' performance at any time. Similar to the integrity of a GNSS-based navigation solution, the most pressing concern in integrity monitoring of a cellular-based navigation solution is the user's ability to recognize when it is safe to use the system.

Integrity monitoring for GNSS-based navigation for AGVs has been studied in the literature. In [16], a framework was proposed to provide integrity provision at the lane-level. The framework warns the user whenever it detects performance anomalies. The method in [16] fuses measurements from a GNSS receiver, an odometer, and a gyroscope with road information through a multiple hypothesis particle filter. The problem of fault detection and isolation in navigation system for passenger vehicles was studied in [17], where the GNSS-based navigation solution is compared with the vehicle's on-board sensors' solution. Then, a sequential statistical test is used to detect discrepancies between the two solutions. The primary differences between the concept of user-level integrity monitoring applied to air transport navigation systems and land vehicle navigation systems was studied in [18]. In [19], a framework to monitor the positioning performance of real-time relative positioning (RRP) systems was proposed, with focus on cooperative intelligent transport systems. The framework considered the state data of the surrounding vehicles obtained from GNSS and dedicated short-range communications (DSRC) units. The monitoring framework provided instantaneous reliability assessment of the RRP systems, which yielded timely alerts to users when the navigation solution cannot be trusted. In [20], an extended Kalman filter (EKF)-based integrity monitoring framework was proposed, which fused data from GNSS and inertial sensors. An interactive multiple model (IMM) method was combined with the EKF-based integrity monitoring framework, to provide position estimates at a meaningful trust-level.

Among several methods developed to monitor a system's integrity, the receiver autonomous integrity monitoring (RAIM) method inherently possesses desirable characteristics, particularly for ground-based receivers in urban canyons, due to its design flexibility and adaptability to the urban environment [21, 22]. In contrast to external integrity monitoring methods, RAIM alleviates the need for costly, bulky, and computationally intensive algorithms in the sense that RAIM detects GNSS pseudorange measurement faults by only exploiting the redundancy of GNSS signals to check the measurements' consistency. RAIM can optionally be coupled with the output of other navigation sensors to improve the integrity monitoring performance [23].

RAIM for the GNSS-based navigation solution is a well-studied topic. However, to the author's knowledge, no research on RAIM for cellular-based navigation has been performed. Research developed over decades for GNSS-based RAIM could serve as a starting point for integrity monitoring of a cellular-based navigation solution. However, GNSS methods do not directly apply to cellular-based navigation integrity monitoring due to fundamental differences between cellular and GNSS signals. First, due to the low elevation angles at which cellular signals are received, cellular signals experience more multipath and signal line-of-sight (LOS) blockage compared to GNSS signals, particularly for ground-based receivers in urban canyons. Second, unlike GNSS-based navigation where the clock error states of GNSS satellites are transmitted in the navigation message, cellular towers do not transmit their clock biases. As such, the clock error states of cellular transmitters must be estimated [24].

This paper proposes a RAIM framework for cellular-based AGV navigation. The framework considers an AGV equipped with a receiver capable of producing pseudorange measurements to nearby cellular towers and an inertial measurement unit (IMU). The tower's locations are assumed to be known (e.g., via signal mapping [24–26]). A detection test is formulated to detect and exclude faulty (i.e., biased) pseudorange measurements and horizontal protection level (HPL) is derived. Experimental results are presented for a ground vehicle navigation in an urban environment (downtown Riverside, California). It is demonstrated that the developed RAIM framework successfully detects and excludes faulty pseudorange measurements, reducing the two-dimensional (2D) position root mean-square

error (RMSE) by 49%.

The paper is organized as follows. Section II describes the AGV's and cellular transmitters' state, the cellular pseudorange measurement model, and the EKF that fuses cellular pseudorange measurements with the AGV's IMU. Section III introduces basic integrity monitoring requirements for AGVs and proposes a RAIM framework to monitor the integrity of the cellular-derived navigation solution. Section IV presents experimental results evaluating the proposed framework in an urban environment with cellular LTE signals. Concluding remarks are provided in Section V.

II. NAVIGATION FRAMEWORK

This section describes the ground vehicle navigation framework. The environment is assumed to comprise N_s terrestrial cellular transmitters, denoted $\{S_n\}_{n=1}^{N_s}$. It is assumed that the vehicle knows the location of the cellular transmitters (e.g., from a local or a cloud-hosted database). This database could be generated *a priori* via several approaches, such as radio mapping (e.g., [24,26]) or satellite images. It is also assumed that the vehicle has an initial period of access to GNSS signals. During this period, the vehicle estimates its state and the cellular transmitters' clock biases. After this period, it is assumed that GNSS signals become unusable, and the vehicle begins to navigate exclusively with cellular signals. The remainder of this section describes the vehicle-mounted receiver clock error dynamics, vehicle's state, and the EKF-based navigation framework.

A. Receiver Clock Error State

The receiver clock error state is given by

$$\boldsymbol{x}_{\text{clk},r} \triangleq \left[c\delta t_r, c\dot{\delta} t_r\right]^{\mathsf{T}},$$

where c is the speed of light, δt_r is the receiver's clock bias, and $\dot{\delta} t_r$ is the receiver's clock drift. The vehicle-mounted receiver clock error state is assumed to evolve according to a double integrator driven by process noise $\tilde{\boldsymbol{w}}_{\text{clk,r}} \triangleq \left[\tilde{w}_{\delta t,r}, \tilde{w}_{\dot{\delta} t,r}\right]^{\mathsf{T}}$, whose elements are modeled as zero-mean, mutually independent white noise processes and the power spectral density of $\tilde{\boldsymbol{w}}_{\text{clk,r}}$ is given by $\tilde{\mathbf{Q}}_{\text{clk,r}} = \text{diag}\left[\text{S}_{\tilde{\text{w}}_{\delta t,\text{r}}}, \text{S}_{\tilde{\text{w}}_{\dot{\delta} t,\text{r}}}\right]$ [27]. The discrete-time equivalent of the clock error dynamics can be expressed as

$$\boldsymbol{x}_{\text{clk},r}(k+1) = \mathbf{F}_{\text{clk}}\boldsymbol{x}_{\text{clk},r}(k) + \boldsymbol{w}_{\text{clk,r}}, \quad \mathbf{F}_{\text{clk}} \triangleq \begin{bmatrix} 1 & T \\ 0 & 1 \end{bmatrix}, \tag{1}$$

where T is the sampling period and $\boldsymbol{w}_{\text{clk,r}}$ is the discrete-time equivalent process noise with covariance $\mathbf{Q}_{\text{clk,r}}$ given by

$$\mathbf{Q}_{\text{clk,r}} = c^2 \begin{bmatrix} S_{\tilde{w}_{\delta t,r}} T + S_{\tilde{w}_{\dot{\delta} t,r}} \frac{T^3}{3} & S_{\tilde{w}_{\dot{\delta} t,r}} \frac{T^2}{2} \\ S_{\tilde{w}_{\dot{\delta} t,r}} \frac{T^2}{2} & S_{\tilde{w}_{\dot{\delta} t,r}} T \end{bmatrix}.$$

B. AGV State

The AGV is assumed to be equipped with:

- an IMU and
- a receiver capable of producing pseudorange measurements to cellular transmitters (e.g., [7,10,28,29]).

If the vehicle is equipped with other navigation sensors (e.g., lidar, camera, etc.), the proposed framework could seamlessly integrate the outputs of these sensors to improve the vehicle's navigation solution. The vehicle's state vector $\boldsymbol{x}_v$ is defined as

$$\boldsymbol{x}_v \triangleq \left[{}^{I}_{G}\bar{\boldsymbol{q}}^{\mathsf{T}} \ , \ {}^{G}\boldsymbol{r}_r^{\mathsf{T}} \ , \ {}^{G}\dot{\boldsymbol{r}}_r^{\mathsf{T}} \ , \ \boldsymbol{b}_g^{\mathsf{T}} \ , \ \boldsymbol{b}_a^{\mathsf{T}} \right]^{\mathsf{T}},$$

where ${}^{I}_{G}\bar{\boldsymbol{q}}$ is the unit quaternion representing the vehicle's orientation (i.e., rotation from the global frame G to the IMU's inertial frame I); ${}^{G}\boldsymbol{r}_r \triangleq [x_r, y_r, z_r]^{\mathsf{T}}$ and ${}^{G}\dot{\boldsymbol{r}}_r$ are the three-dimensional (3-D) position and velocity of the vehicle, respectively expressed in G; and $\boldsymbol{b}_g$ and $\boldsymbol{b}_a$ are the gyroscope and accelerometer biases, respectively. Standard IMU state time update model can be used to propagate the states of the IMU [30–33].

C. EKF Prediction Error Covariance Time Update

This subsection discusses calculation of the prediction error covariance time update. The EKF estimates the state vector $\boldsymbol{x}$ consisting of the vehicle's and the receiver's clock error states simultaneously, i.e., $\boldsymbol{x} \triangleq \left[\boldsymbol{x}_v^{\mathsf{T}}, \boldsymbol{x}_{\text{clk,r}}^{\mathsf{T}}\right]^{\mathsf{T}}$. Denote

$$\hat{\boldsymbol{x}}(k|j) \triangleq \left[{}^{I_{k|j}}_{G}\hat{\bar{\boldsymbol{q}}}^{\mathsf{T}}, {}^{G}\hat{\boldsymbol{r}}_r^{\mathsf{T}}(k|j), {}^{G}\hat{\dot{\boldsymbol{r}}}_r^{\mathsf{T}}(k|j),\ \hat{\boldsymbol{b}}_g^{\mathsf{T}}(k|j), \hat{\boldsymbol{b}}_a^{\mathsf{T}}(k|j), \hat{\boldsymbol{x}}_{\text{clk,r}}^{\mathsf{T}}(k|j)\right]^{\mathsf{T}},$$

as the state estimate produced by the EKF at time-step k, which is obtained using all measurements (IMU and cellular pseudorange) from time-step 1 to $j \leq k$. Note that the quaternion representation is an over-determined representation of the orientation of the vehicle. Hence, the estimation error covariance associated with the quaternion estimate will always be singular. To avoid singularity, the 3-axis angle error vector $\tilde{\boldsymbol{\theta}} \in \mathbb{R}^3$ is used to form the orientation error state vector. Denote $\hat{\bar{\boldsymbol{q}}}$ as the estimate of $\bar{\boldsymbol{q}}$ and the error quaternion as $\delta\bar{\boldsymbol{q}}$, then, the orientation error model follows the quaternion multiplication model given by,

$$\bar{\boldsymbol{q}} = \delta\bar{\boldsymbol{q}} \otimes \hat{\bar{\boldsymbol{q}}}, \qquad \delta\bar{\boldsymbol{q}} \simeq \left[\frac{1}{2}\tilde{\boldsymbol{\theta}}^{\mathsf{T}},\ \sqrt{1 - \frac{1}{4}\tilde{\boldsymbol{\theta}}^{\mathsf{T}}\tilde{\boldsymbol{\theta}}}\right]^{\mathsf{T}}, \tag{2}$$

where $\otimes$ is the quaternion multiplication operator. The vehicle's and receiver's clock error states are defined using the standard additive error model (i.e., $\tilde{\boldsymbol{v}} \triangleq \boldsymbol{v} - \hat{\boldsymbol{v}}$). Therefore, the prediction error vector at time-step k in the EKF is expressed as

$$\tilde{\boldsymbol{x}}(k|j) \triangleq \left[\tilde{\boldsymbol{\theta}}^{\mathsf{T}}(k|j)\ ,\ {}^{G}\tilde{\boldsymbol{r}}_r^{\mathsf{T}}(k|j)\ ,\ {}^{G}\tilde{\dot{\boldsymbol{r}}}_r^{\mathsf{T}}(k|j),\quad \tilde{\boldsymbol{b}}_g^{\mathsf{T}}(k|j)\ ,\ \tilde{\boldsymbol{b}}_a^{\mathsf{T}}(k|j)\ ,\ \tilde{\boldsymbol{x}}_{\text{clk,r}}^{\mathsf{T}}(k|j)\right]^{\mathsf{T}},$$

with the associated prediction error covariance $\mathbf{P}(k|j)$. Details of this prediction error model can be found in [33–36].

D. EKF Measurement Model

After discretization and mild approximations, the pseudorange made by the vehicle-mounted receiver on the n-th cellular transmitter at the k-th time-step can be shown to be

$$z_{s_n}(k) = \left\|{}^{G}\boldsymbol{r}_r(k) - \boldsymbol{r}_{s_n}\right\|_2 + c\left[\delta t_r(k) - \delta t_{s_n}(k)\right] + v_{s_n}(k), \tag{3}$$

where $\boldsymbol{r}_{s_n} \triangleq [x_{s_n}, y_{s_n}, z_{s_n}]^{\mathsf{T}}$ is the location of the n-th cellular transmitter, δt_{s_n} is the clock bias of the n-th cellular transmitter, and v_{s_n} is the measurement noise, which is modeled as a DT zero-mean white Gaussian sequence with variance $\sigma_{s_n}^2$ [37]. The clock biases $\{\delta t_{s_n}\}_{n=1}^{N_s}$ are modeled as a first-order polynomials [38, 39], i.e., $\delta t_{s_n}(k) = \dot{\delta} t_{s_n} kT + \delta t_{s_n,0}$, where $\dot{\delta} t_{s_n}$ is the constant clock drift of the n-th cellular transmitter and $\delta t_{s_n,0}$ is the corresponding initial bias. The coefficients $\left\{\dot{\delta} t_{s_n}, \delta t_{s_n,0}\right\}_{n=1}^{N_s}$ are calculated during the period when GNSS signals are available. These values can be calculated with knowledge of the vehicle's position and its receiver's clock bias (cf. (3)) by solving a least-square (LS) estimation problem. The vector of pseudorange measurements to all N_s cellular transmitters is given by

$$\boldsymbol{z} = \left[z_{s_1}, \ldots, z_{s_{N_s}}\right]^{\mathsf{T}}, \tag{4}$$

and it is assumed that the measurement noise $\{v_{s_n}\}_{n=1}^{N_s}$ are independent.

E. EKF State and Covariance Measurement Update

The state measurement update $\hat{\boldsymbol{x}}(k+1|k+1)$ and associated estimation error covariance $\mathbf{P}(k+1|k+1)$ are computed using standard EKF update equations [31], except for the orientation state which is updated according to the

quaternion error model [35]. The corresponding measurement Jacobian $\mathbf{H}$ is given by

$$\mathbf{H} = [\,\mathbf{H}_v,\, \mathbf{H}_{\text{clk}}\,],$$

where,

$$\mathbf{H}_v \triangleq \begin{bmatrix} \mathbf{0}_{1\times 3} & \mathbf{1}_{s_1}^{\mathsf{T}} & \mathbf{0}_{1\times 9} \\ \vdots & \vdots & \vdots \\ \mathbf{0}_{1\times 3} & \mathbf{1}_{s_{N_s}}^{\mathsf{T}} & \mathbf{0}_{1\times 9} \end{bmatrix},\ \mathbf{1}_{s_n} \triangleq \frac{{}^{G}\hat{\boldsymbol{r}}_r(k+1|j) - \boldsymbol{r}_{s_n}}{\|{}^{G}\hat{\boldsymbol{r}}_r(k+1|j) - \boldsymbol{r}_{s_n}\|_2},\quad \mathbf{H}_{\text{clk}} \triangleq [\mathbf{h}_{\text{clk}} \quad \dots \quad \mathbf{h}_{\text{clk}}]^{\mathsf{T}},\quad \mathbf{h}_{\text{clk}} \triangleq [1 \quad 0]^{\mathsf{T}}.$$

The measurement noise covariance takes the form

$$\mathbf{R} = \text{diag}\left[\sigma_{\text{s}_1}^2, \dots, \sigma_{\text{s}_{\text{N}_\text{s}}}^2\right].$$

III. RAIM FOR CELLULAR-BASED NAVIGATION

RAIM is an integrity monitoring technique based on consistency check of redundancy of range measurements. It consists of two main stages:

Stage 1: Performs a fault detection test to detect performance anomalies and to distinguish between fault-free and faulty operations.
Stage 2: Provides a horizontal protection level (HPL), which is the statistical error bound that guarantees that the probability of the absolute position error exceeding a pre-defined threshold is smaller than or equal to the target integrity risk [40].

The target integrity risk refers to the maximum probability with which a receiver is allowed to provide position failures not detected by the integrity monitoring system [41]. This section, outlines the fault detection steps and describes the steps to compute the HPL for cellular-based navigation.

A. Fault Detection Test

A faulty operation occurs when a bias with magnitude b_n is injected into the pseudorange measurement drawn from the n-th cellular transmitter. This could be due to a cellular transmitter failure, signal LOS blockage, or high signal attenuation. In this section, a maximum of only one fault at each time-step is considered. In order to distinguish between fault-free and faulty operations, a measurable scalar parameter is defined that provides information about pseudorange measurement errors. This parameter, called a test statistic φ, is a random variable with a known distribution.

The test statistic is generated using the normalized innovation squared (NIS) [42] according to

$$\varphi(k+1) = \boldsymbol{\nu}^{\mathsf{T}}(k+1)\mathbf{S}^{-1}(k+1)\boldsymbol{\nu}(k+1),$$

where the innovation vector $\boldsymbol{\nu}$ and its corresponding covariance matrix $\mathbf{S}$ are computed from

$$\begin{aligned} \boldsymbol{\nu}(k+1) &= \boldsymbol{z}(k+1) - \hat{\boldsymbol{z}}(k+1|j) \\ \mathbf{S}(k+1) &= \mathbf{H}(k+1)\mathbf{P}(k+1|j)\mathbf{H}^{\mathsf{T}}(k+1) + \mathbf{R}(k). \end{aligned}$$

NIS-based test statistics follow a chi-square distribution in a fault-free operation and a non-central chi-square distribution in faulty operations [42]. The degrees of freedom d of the distributions in both fault-free and faulty operations is $d = N_s - 4$, and the non-centrality parameter in a faulty operation is given by

$$\lambda(k+1) = {\boldsymbol{u}_n}^{\mathsf{T}}(k+1)\mathbf{S}^{-1}(k+1)\boldsymbol{u}_n(k+1),$$

where the vector $\boldsymbol{u}_n(k+1) \triangleq [0, \dots, 0, b_n(k+1), 0, \dots, 0]^{\mathsf{T}}$ indicates the faulty cellular transmitter along with the magnitude of the bias in the pseudorange measurement drawn from the faulty cellular transmitter. The fault detection is achieved by comparing the test statistic against the detection threshold T_h, i.e.,

$$\begin{aligned} &\varphi(k+1) \le T_h : \text{no fault detected,} \\ &\varphi(k+1) > T_h : \text{fault detected.} \end{aligned}$$

The value of T_h is obtained using a given probability of false alarm, P_{FA}, under a fault-free operation according to

$$P_{\text{FA}} = \int_{T_h}^{\infty} f_{\chi^2_d}(\tau) d\tau, \tag{5}$$

where $f_{\chi^2_d}$ is the probability density function (pdf) of the chi-square distribution with d degrees of freedom. The value of T_h can be obtained from a chi-square cumulative density function (cdf) table using P_{FA} and d.

B. Horizontal Protection Level

For each estimated position, RAIM provides HPL, a circular area centered at the user's real position, which is assured to contain the estimated position with a probability equal or higher than $1 - P_{\text{MD}}$, where P_{MD} is the probability of missed detection [43]. The decision of alert is done by comparing the HPL and a specified horizontal alert limit (HAL), which is the largest position error allowable for a safe operation, i.e.,

$$\begin{aligned} &\text{HPL} > \text{HAL} : \text{the alarm triggers,} \\ &\text{HPL} \leq \text{HAL} : \text{the alarm does not trigger.} \end{aligned}$$

The non-centrality parameter of the chi-square distribution under a faulty operation that results in a missed detection rate P_{MD} is denoted λ_{min}. Given a desired P_{MD} as a design parameter and T_h obtained from (5), λ_{min} is computed according to

$$P_{\text{MD}} = \int_{0}^{T_h} f_{\chi^2_d, \lambda_{\text{min}}}(\tau) d\tau, \tag{6}$$

where $f_{\chi^2_d, \lambda_{\text{min}}}$ represents the pdf of the non-central chi-square distribution with d degrees of freedom and non-centrality parameter λ_{min}. The value of λ_{min} can be obtained from a chi-square cdf table.

Next, a parameter called slope_n is introduced to project the bias in the faulty measurement onto the horizontal position error domain. A recursive derivation for slope_n is calculated using the EKF update equation according to

$$\boldsymbol{\Delta x}_{\text{err},n}(k+1) \approx \boldsymbol{\Xi}(k+1)\boldsymbol{u}_n(k+1),$$

where $\boldsymbol{\Delta x}_{\text{err},n}$ is the additive bias in the error states and

$$\begin{aligned} \boldsymbol{\Xi}(k+1) &= \mathbf{M}(k+1)\boldsymbol{\Xi}(k) + \mathbf{K}(k+1) \\ \boldsymbol{\Xi}(1) &= \mathbf{K}(1), \end{aligned}$$

where $\mathbf{K}$ is the Kalman gain and

$$\mathbf{M}(k+1) \triangleq [\mathbf{I} - \mathbf{K}(k+1)\mathbf{H}(k+1)]\mathbf{F}.$$

Since the fault in the measurement is being projected onto the horizontal plane, only the fourth and fifth rows of $\boldsymbol{\Xi}(k+1)$ (i.e., x- and y- directions in the global frame) are used to construct slope_n. Subsequently, slope_n is expressed as

$$\text{slope}_n(k+1) = \frac{\Delta r_{\text{err},n}(k+1)}{\sqrt{(\mathbf{S}^{-1}(k+1))_{n,n}}},$$

where $(\mathbf{S}^{-1})_{n,n}$ indicates the n-th diagonal element of matrix $\mathbf{S}^{-1}$ and

$$\Delta r_{\text{err},n}(k+1) = \sqrt{[(\boldsymbol{\Xi}(k+1))_{4,n}]^2 + [(\boldsymbol{\Xi}(k+1))_{5,n}]^2}.$$

The HPL is calculated as the projection onto the horizontal position domain of the pseudorange measurement bias that generates a non-centrality parameter equal to λ_{min} in the cellular transmitter with the maximum slope [41], i.e.,

$$\text{HPL}(k+1) = \text{slope}_{\text{max}}(k+1)\sqrt{\lambda_{\text{min}}},$$

where

$$\text{slope}_{\max}(k+1) = \max_{n} \{\text{slope}_n(k+1)\}, \quad n = 1, \ldots, N_s.$$

Similar to GNSS-based RAIM [40], fault exclusion in cellular-based RAIM is performed by constructing N_s subsets of $N_s - 1$ pseudorange measurements. Assuming that only one of the cellular transmitters is faulty, applying the fault detection procedure described above to each subset will result in a fault in all subsets except the one from which the faulty cellular transmitter's pseudorange measurement is excluded. Fig. 1 demonstrates a step-by-step summary of the proposed cellular-based RAIM technique.

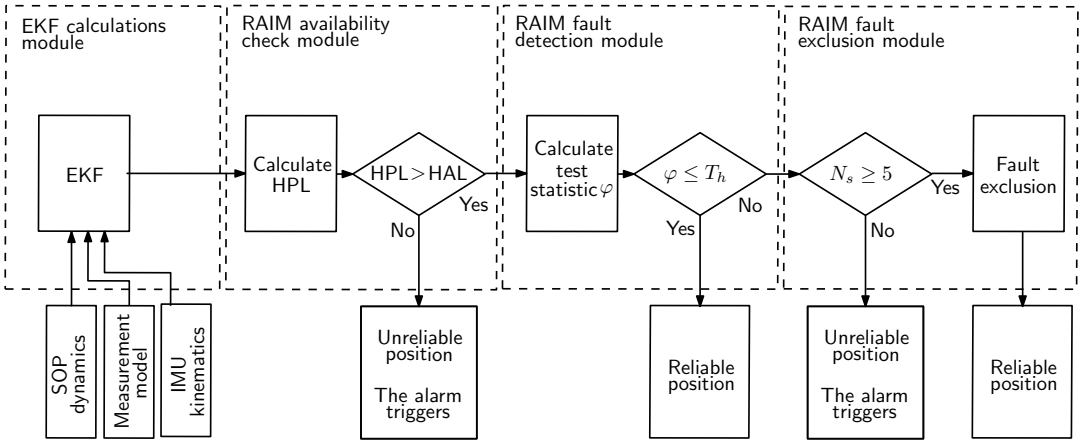

Fig. 1. Step-by-step summary of the proposed cellular-based RAIM technique. The proposed method consists of four parts: EKF calculations, availability check, fault detection, and fault exclusion.

IV. EXPERIMENTAL RESULTS

A field test was conducted to validate the proposed framework on a ground vehicle navigation in an urban environment (downtown Riverside, California). This section presents the hardware used in this experiment along with the experimental results.

A. Experimental Hardware Setup and Scenario Description

A vehicle was equipped with an integrated AsteRx-i V GPS-IMU sensor [44] whose x-axis points toward the front of the vehicle, z-axis points upward, and y-axis points to the right side of the ground vehicle. The IMU returns six measurements (accelerations and rotational rates along the three orthogonal axes of the body frame) at a rate of 100 Hz. Over the course of the experiment, the ground-truth trajectory of the vehicle was obtained from its integrated GPS-IMU navigation system, while the IMU accelerations and rotational rates outputs were used to propagate the states. Septentrio's post-processing software development kit (PP-SDK) was used to process carrier phase observables collected by the AsteRx-i V and by a nearby differential GPS base station to obtain a carrier phase-based navigation solution. This integrated GNSS-IMU real-time kinematic (RTK) system was used to produce the ground-truth results with which the proposed navigation framework was compared. The ground vehicle was also equipped with two cellular antennas to acquire and track signals from nearby cellular LTE towers. The LTE antennas used for the experiment were consumer-grade 800/1900 MHz cellular antennas. The signals were simultaneously down-mixed and synchronously sampled via a National Instruments (NI) dual-channel universal software radio peripheral (USRP)–2954R, driven by a GPS-disciplined oscillator (GSPDO). The clock bias and drift process noise power spectral densities of the receiver were set to be 1.3×10^{-22} s and 7.89×10^{-25} 1/s respectively, since the 2954R USRPs are equipped with oven-controlled crystal oscillators (OCXOs). The receiver was tuned to carrier frequencies of 1955 MHz and 739 MHz, which are channels allocated for U.S. cellular provider AT&T. Samples of the received signals were stored for off-line post-processing. The Multichannel Adaptive TRansceiver Information eXtractor (MATRIX) software-defined receiver (SDR) developed in [45] was used to produce LTE pseudoranges.

Fig. 2 illustrates the experimental hardware setup and traversed trajectory. The cellular transmitters' clock biases $\{\delta t_{s_n}\}_{n=1}^{N_s}$ were calculated according to the first-order polynomials model discussed in Subsection II-D. The initial

clock bias and constant clock drift $\left\{\delta t_{s_n,0}, \dot{\delta} t_{s_n}\right\}_{n=1}^{N_s}$ were calculated during an initial period of GNSS availability. Moreover, during the period of GNSS availability, the vehicle's orientation ${}^{I}_{G}\bar{\boldsymbol{q}}$, position ${}^{G}\boldsymbol{r}_r$, velocity ${}^{G}\dot{\boldsymbol{r}}_r$, and its clock error states $\boldsymbol{x}_{\text{clk},r}$ were estimated along with their corresponding covariance, which were used to initialize the EKF. The gyroscope's and accelerometer's biases were initialized by taking the mean of 5 seconds of IMU data, when the receiver was stationary. The measurement noise variances were determined empirically.

Fig. 2. Experimental hardware setup and the traversed trajectory along with the position of cellular LTE towers. A ground vehicle was equipped with an integrated AsteRx-i V GPS-IMU sensor, cellular antennas, and USRPs. The ground vehicle traveled 1.35 km in an urban area (downtown Riverside, California) collecting GPS, IMU measurements, and cellular LTE signals from five cellular towers.

B. Experimental Results

The fault detection test and HPL calculations were performed throughout the experimental test. The results are shown in Fig. 3. Fig. 3 (a) shows the fault detection test, which compares the test statistic φ against the detection threshold T_h. It can be seen that at $t = 25$ s, the threshold is exceeded; therefore, the test is not declared successful (see the red circle in Fig. 3 (a)). This implies that at least one of the measurements was faulty and its contribution to the test statistic was significant enough for the test to fail. The fault exclusion technique indicated that the faulty measurement was the pseudorange drawn from the first cellular LTE tower. The 2D position RMSE of the navigation solution without measurement exclusion was 6.8 m, while the 2D position RMSE with the developed RAIM framework was 3.5 m. Hence, incorporating the developed RAIM framework in this paper reduced the position RMSE by 49%. Fig. 3(b)–(c) show the position estimation error with and without fault exclusion.

Fig. 4 illustrates the HPL and HAL. In contrast to weighted least-square (WLS)-based RAIM [43] where the HPL does not depend on the current measurements and can be predicted according to the expected satellite/user geometry, the HPL in the proposed RAIM method depends on both the current states and measurements. Therefore, it must be calculated at each time-step. As can be seen, over the course of the experiment, HPL does not exceed HAL. Subsequently, RAIM was available throughout the experiment, which means that RAIM was able to detect the presence of the faults within the required P_{MD}.

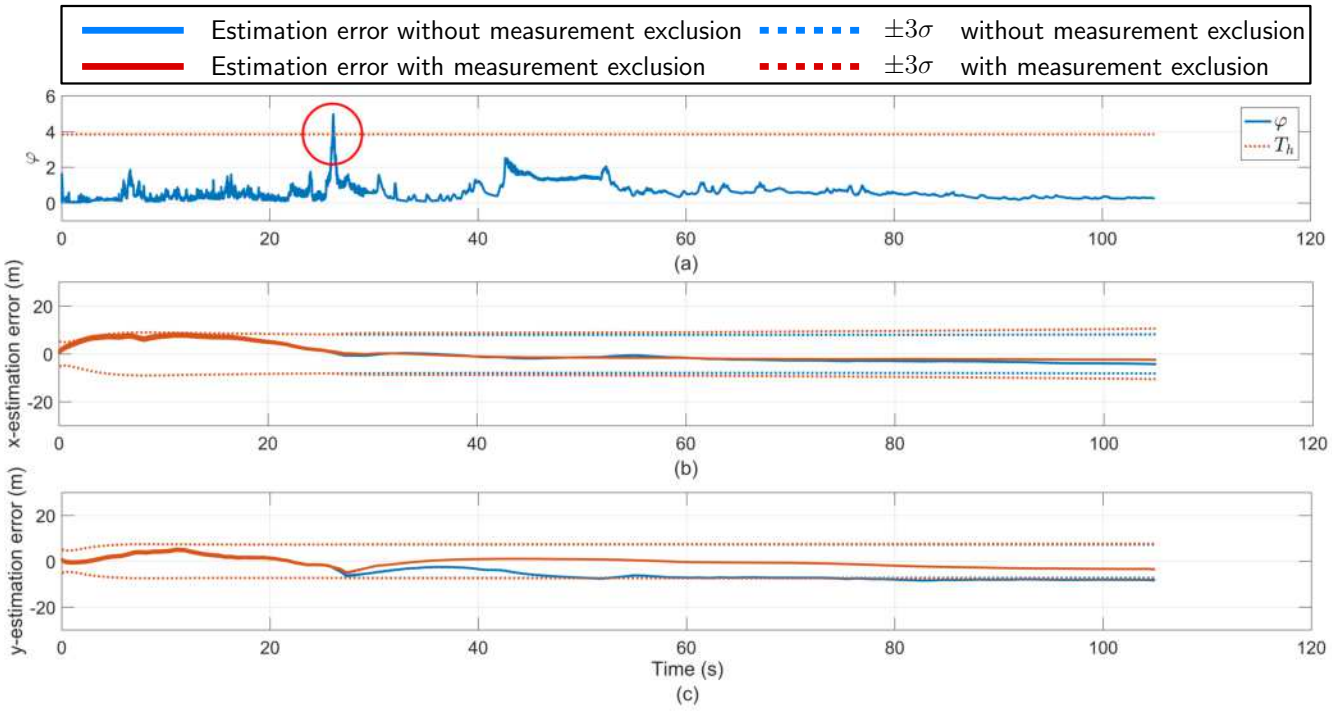

Fig. 3. The resulting (a) test statistic and (b)–(c) position estimation error with and without measurement exclusion in the x- and y-directions.

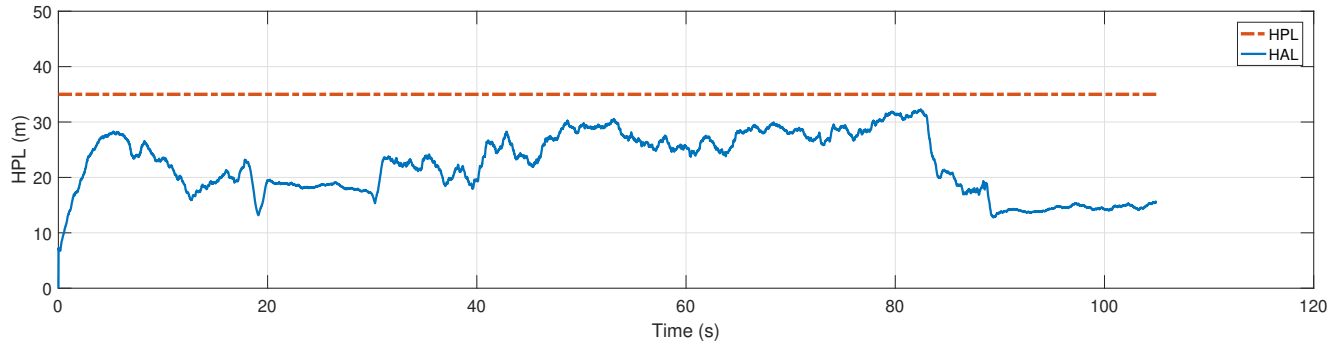

Fig. 4. The HPL and HAL over the course of the experiment

V. CONCLUSION

In this paper, a framework for AGV integrity monitoring in GNSS-challenged environment was developed. To this end, an EKF-based RAIM technique was proposed, which used an IMU and pseudoranges extracted from ambient cellular LTE towers. The proposed RAIM framework detects and excludes faulty measurements and calculates the HPL. Experimental results over a total traversed trajectory of 1.35 km validated the efficacy of the proposed framework and showed that the proposed RAIM-based measurement exclusion technique reduced the 2D position RMSE by 49%.

ACKNOWLEDGMENT

The authors would like to thank Kimia Shamaei, Sonya Ragothaman, and Joshua Morales for their help with the data collection. This work was supported in part by the National Science Foundation (NSF) under Grant 1751205 and the Office of Naval Research (ONR) under Grant N00014-16-1-2305 and Grant N00014-16-1-2809.

References

[1] S. Ji, W. Chen, X. Ding, Y. Chen, C. Zhao, and C. Hu, "Potential benefits of GPS/GLONASS/GALILEO integration in an urban canyon – Hong Kong," *Journal of Navigation*, vol. 63, no. 4, pp. 681–693, October 2010.

[2] D. Borio, F. Dovis, H. Kuusniemi, and L. L. Presti, "Impact and detection of GNSS jammers on consumer grade satellite navigation receivers," *Proceedings of the IEEE*, vol. 104, no. 6, pp. 1233–1245, February 2016.

[3] K. Fisher, "The navigation potential of signals of opportunity-based time difference of arrival measurements," Ph.D. dissertation, Air Force Institute of Technology, Wright-Patterson Air Force Base, Ohio, USA, 2005.

[4] J. Raquet and R. Martin, "Non-GNSS radio frequency navigation," in *Proceedings of IEEE International Conference on Acoustics, Speech and Signal Processing*, March 2008, pp. 5308–5311.

[5] Z. Kassas, "Collaborative opportunistic navigation," *IEEE Aerospace and Electronic Systems Magazine*, vol. 28, no. 6, pp. 38–41, 2013.

[6] Z. Kassas, "Analysis and synthesis of collaborative opportunistic navigation systems," Ph.D. dissertation, The University of Texas at Austin, USA, 2014.

[7] Z. Kassas, J. Khalife, K. Shamaei, and J. Morales, "I hear, therefore I know where I am: Compensating for GNSS limitations with cellular signals," *IEEE Signal Processing Magazine*, pp. 111–124, September 2017.

[8] K. Shamaei, J. Khalife, S. Bhattacharya, and Z. Kassas, "Computationally efficient receiver design for mitigating multipath for positioning with LTE signals," in *Proceedings of ION GNSS Conference*, September 2017, pp. 3751–3760.

[9] K. Shamaei and Z. Kassas, "LTE receiver design and multipath analysis for navigation in urban environments," *NAVIGATION, Journal of the Institute of Navigation*, 2018, accepted.

[10] C. Yang, T. Nguyen, and E. Blasch, "Mobile positioning via fusion of mixed signals of opportunity," *IEEE Aerospace and Electronic Systems Magazine*, vol. 29, no. 4, pp. 34–46, April 2014.

[11] M. Driusso, C. Marshall, M. Sabathy, F. Knutti, H. Mathis, and F. Babich, "Vehicular position tracking using LTE signals," *IEEE Transactions on Vehicular Technology*, vol. 66, no. 4, pp. 3376–3391, April 2017.

[12] J. Khalife and Z. Kassas, "Navigation with cellular CDMA signals – part II: Performance analysis and experimental results," *IEEE Transactions on Signal Processing*, vol. 66, no. 8, pp. 2204–2218, April 2018.

[13] J. Khalife and Z. Kassas, "Precise UAV navigation with cellular carrier phase measurements," in *Proceedings of IEEE/ION Position, Location, and Navigation Symposium*, April 2018, pp. 978–989.

[14] J. Khalife, K. Shamaei, S. Bhattacharya, and Z. Kassas, "Centimeter-accurate UAV navigation with cellular signals," in *Proceedings of ION GNSS Conference*, September 2018, accepted.

[15] M. Maaref, J. Khalife, and Z. Kassas, "Lane-level localization and mapping in GNSS-challenged environments by fusing lidar data and cellular pseudoranges," *IEEE Transactions on Intelligent Vehicles*, 2018, accepted.

[16] R. Toledo-Moreo, D. Betaille, and F. Peyret, "Lane-level integrity provision for navigation and map matching with GNSS, dead reckoning, and enhanced maps," *IEEE Transactions on Intelligent Transportation Systems*, vol. 11, no. 1, pp. 100–112, March 2010.

[17] C. Zinoune, P. Bonnifait, and J. Ibanez-Guzman, "Sequential FDIA for autonomous integrity monitoring of navigation maps on board vehicles," *IEEE Transactions on Intelligent Transportation Systems*, vol. 17, no. 1, pp. 143–155, January 2016.

[18] N. Velaga, M. Quddus, A. Bristow, and Y. Zheng, "Map-aided integrity monitoring of a land vehicle navigation system," *IEEE Transactions on Intelligent Transportation Systems*, vol. 13, no. 2, pp. 848–858, June 2012.

[19] K. Ansari, Y. Feng, and M. Tang, "A runtime integrity monitoring framework for real-time relative positioning systems based on GPS and DSRC," *IEEE Transactions on Intelligent Transportation Systems*, vol. 16, no. 2, pp. 980–992, April 2015.

[20] R. Toledo-Moreo, M. Zamora-Izquierdo, B. Ubeda-Miarro, and A. Gomez-skarmeta, "High-integrity IMM-EKF-based road vehicle navigation with low-cost GPS/SBAS/INS," *IEEE Transactions on Intelligent Transportation Systems*, vol. 8, no. 3, pp. 491–511, September 2007.

[21] L. Zhang, J. Li, T. Cui, and S. Liu, "An adapted RAIM algorithm for urban canyon environment," in *Proceedings of Cooperative Positioning and Service*, May 2017, pp. 116–121.

[22] D. Salos, "Integrity monitoring applied to the reception of GNSS signals in urban environments," Ph.D. dissertation, National Polytechnic Institute of Toulouse, University of Toulouse, Toulouse, France, 2012.

[23] S. Khanafseh, N. Roshan, S. Langel, F. Chan, M. Joerger, and B. Pervan, "GPS spoofing detection using RAIM with INS coupling," in *Proceedings of IEEE/ION Position, Location, and Navigation Symposium*, May 2014, pp. 1232–1239.

[24] Z. Kassas, V. Ghadiok, and T. Humphreys, "Adaptive estimation of signals of opportunity," in *Proceedings of ION GNSS Conference*, September 2014, pp. 1679–1689.

[25] J. Morales and Z. Kassas, "Optimal receiver placement for collaborative mapping of signals of opportunity," in *Proceedings of ION GNSS Conference*, September 2015, pp. 2362–2368.

[26] J. Morales and Z. Kassas, "Optimal collaborative mapping of terrestrial transmitters: receiver placement and performance characterization," *IEEE Transactions on Aerospace and Electronic Systems*, vol. 54, no. 2, pp. 992–1007, April 2018.

[27] J. Barnes, A. Chi, R. Andrew, L. Cutler, D. Healey, D. Leeson, T. McGunigal, J. Mullen, W. Smith, R. Sydnor, R. Vessot, and G. Winkler, "Characterization of frequency stability," *IEEE Transactions on Instrumentation and Measurement*, vol. 20, no. 2, pp. 105–120, May 1971.

[28] J. del Peral-Rosado, J. Lopez-Salcedo, G. Seco-Granados, F. Zanier, P. Crosta, R. Ioannides, and M. Crisci, "Software-defined radio LTE positioning receiver towards future hybrid localization systems," in *Proceedings of International Communication Satellite Systems Conference*, October 2013, pp. 14–17.

[29] J. del Peral-Rosado, R. Raulefs, J. Lpez-Salcedo, and G. Seco-Granados, "Survey of cellular mobile radio localization methods: from 1G to 5G," *IEEE Communications Surveys & Tutorials*, vol. 20, no. 2, pp. 1124–1148, 2018.

[30] J. Farrell and M. Barth, *The Global Positioning System and Inertial Navigation*. New York: McGraw-Hill, 1998.

[31] Y. Bar-Shalom, X. Li, and T. Kirubarajan, *Estimation with Applications to Tracking and Navigation*. New York, NY: John Wiley & Sons, 2002.

[32] P. Groves, "The PNT boom: future trends in integrated navigation," *Inside GNSS*, pp. 44–49, March/April 2013.

[33] J. Morales, P. Roysdon, and Z. Kassas, "Signals of opportunity aided inertial navigation," in *Proceedings of ION GNSS Conference*, September 2016, pp. 1492–1501.

[34] P. Groves, *Principles of* GNSS*, Inertial, and Multisensor Integrated Navigation Systems*, 2nd ed. Artech House, 2013.

[35] M. Shelley, "Monocular visual inertial odometry," Master's thesis, Technical University of Munich, Germany, 2014.

[36] J. Morales, J. Khalife, and Z. Kassas, "Collaborative autonomous vehicles with signals of opportunity aided inertial navigation systems," in *Proceedings of ION International Technical Meeting Conference*, January 2017, 805–818.

[37] Z. Kassas and T. Humphreys, "Observability analysis of collaborative opportunistic navigation with pseudorange measurements," *IEEE Transactions on Intelligent Transportation Systems*, vol. 15, no. 1, pp. 260–273, February 2014.
[38] F. Knutti, M. Sabathy, M. Driusso, H. Mathis, and C. Marshall, "Positioning using LTE signals," in *Proceedings of Navigation Conference in Europe*, April 2015, pp. 1–8.
[39] K. Shamaei, J. Khalife, and Z. Kassas, "Performance characterization of positioning in LTE systems," in *Proceedings of ION GNSS Conference*, September 2016, pp. 2262–2270.
[40] N. Zhu, J. Marais, D. Betaille, and M. Berbineau, "GNSS position integrity in urban environments: A review of literature," *IEEE Transactions on Intelligent Transportation Systems*, vol. PP, no. 99, pp. 1–17, January 2018.
[41] D. Salos, C. Macabiau, A. Martineau, B. Bonhoure, and D. Kubrak, "Analysis of GNSS integrity requirements for road user charging applications," in *Proceedings of Satellite Navigation Technologies and European Workshop on GNSS Signals and Signal Processing*, December 2010, pp. 1–8.
[42] A. Grosch, O. G. Crespillo, I. Martini, and C. Gunther, "Snapshot residual and Kalman filter based fault detection and exclusion schemes for robust railway navigation," in *Proceedings of European Navigation Conference*, May 2017, pp. 36–47.
[43] D. Salos, A. Martineau, C. Macabiau, B. Bonhoure, and D. Kubrak, "Receiver autonomous integrity monitoring of GNSS signals for electronic toll collection," *IEEE Transactions on Intelligent Transportation Systems*, vol. 15, no. 1, pp. 94–103, February 2014.
[44] (2018) Septentrio AsteRx-i V. [Online]. Available: https://www.septentrio.com/products
[45] K. Shamaei, J. Khalife, and Z. Kassas, "Exploiting LTE signals for navigation: Theory to implementation," *IEEE Transactions on Wireless Communications*, vol. 17, no. 4, pp. 2173–2189, April 2018.